2008 IEEE International Conference on
Robotics and Automation
Pasadena, CA, USA, May 19-23, 2008

# Development of a new linear actuator for Androids

Masayuki MISHIMA, Hiroshi ISHIGURO and Katsuhiro HIRATA, *Member, IEEE*

***Abstract*— In order to realize androids and humanoids that have very humanlike mechanisms and movements, the development of new linear actuators is necessary. In the development of the actuators, we have found a structure of the linear actuator that is more powerful and quick through iterative simulations based on the 3D finite element method and developed the prototype. This paper reports the structure and various simulations of the new linear actuator. We consider this new actuator will be one of the important components of robots, such as androids and humanoids.**

## I. INTRODUCTION

INTERACTION has been one of the important issues in robotics in addition to navigation and manipulation. Robots are expected to work in our daily environment and support human activities. For realizing the interactive behaviors, the robot needs to have more humanlike mechanism and behaviors.

As such a humanlike robot, we have built several android robots and one of them is shown as an example in Fig. 1 [1]. The main difference between mechanical-looking robots and the androids is the natural humanlike movements in addition to the humanlike appearance. For realizing the humanlike movements, we have developed the complicated mechanism of the android by using pneumatic actuators as shown in Fig. 2.

For the mechanism, the actuator is the key component. Normally, DC servo motors that are compact and battery-powered are used. Almost all of humanoids are developed by using the DC servo motors. However, it requires reduction gears. For example, elbow parts of Wakamaru which is developed by MITSUBISHI HEAVY INDUSTRIES, LTD. are equipped with coreless motors and reduction gears. They make unnatural noise as an android. Further, it does not have humanlike compliance and back drivability. Therefore, we have used pneumatic actuators for the android.

The android has 42 pneumatic actuators for the upper torso except fingers. For example, the right figure in Fig. 3 shows the android's arm that has two pneumatic linear actuators. The actuators that we are using are as follows:

*Rotary pneumatic actuator*
*HI-ROTER, KURODA Pneumatics Ltd.*
*(http://kuroda-precision.co.jp/KPL/english/index.html)*
*Linear pneumatic actuator*
*Air Cylinder, SMC Corporation(http://www.smcusa.com/)*

Manuscript received April 9, 2007.

H. Ishiguro, M. Mishima, and K. Hirata are with Department of Adaptive Machine Systems, Graduate School of Engineering, Osaka University, Osaka, JAPAN (phone: +81-6-6879-4180; fax: +81-6-6879-4180; e-mail: masayuki.mishima@ams.eng.osaka-u.ac.jp).

Fig. 1. Photograph of an android

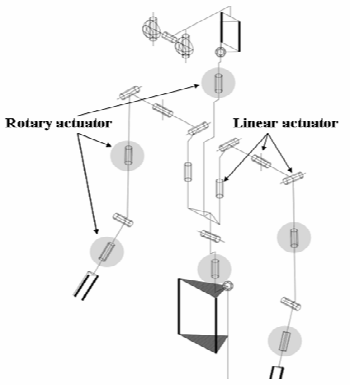


Fig. 2. The arrangement of actuators

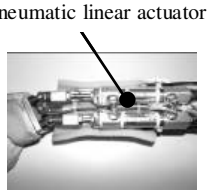


Fig. 3. Arm composed of pneumatic linear actuator.

The output power is decided by the diameter of the air cylinder and the air pressure provided by the air compressor. The linear pneumatic actuators are as follows.

*SMC CJ2B16-10-DCH185FH*
*Diameter: 16 mm*
*Stroke: 10 mm*
*Maximum operating pressure: 0.7M Pa*
*Maximum output: 140 N*

However, the pneumatic actuators have several demerits. For example, it requires a large and powerful air compressor and the control is difficult. Therefore, we have designed new cylindrical electromagnetic linear actuators for replacing with them. The requirements for the new actuators are as follows:

a) No necessity of the large air compressor
b) No gear noise
c) Long stroke
d) Higher response
e) Controllable compliance

For developing cylindrical electromagnetic linear actuators that satisfy these requirements, we have iteratively simulated various arrangement of the magnet and structure of the

actuators by our code (3-D FEM) [2]. And finally, we have found a new structured linear actuator. The basic idea is to utilize Halbach array [3, 4] for the linear actuators. Halbach array is a well-known magnet arrangement; however, it has not been used for linear actuators so far. We could develop a linear actuator that is more than 30% better in the thrust and more than 40% better in the response comparing with a shaft motor that is the most powerful linear actuator. We believe this actuator improves the robot performance and develops their various practical applications.

In the remaining sections, this paper reports the basic structure and the operating principle. We have optimized the structure of the linear actuator by combining the excitation analysis by the 3-D FEM and the motion equations. Further, we have verified the performance by building prototypes and compared with the shaft motor.

## II. The Liner Actuator and The Operating Principle

### A. The Basic Structure

The half model of the proposed cylindrical liner actuator is shown in Fig. 4. The mover is mainly composed of the magnet block and non-magnetic shaft. The magnet block consists of four magnets with different magnetization directions at an interval of 90degrees. The magnet arrangement, called Halbach array (see Fig. 5), can generate the high magnetic flux in the outside of the mover.

The magnetization of the magnet (NdFeB) is 1.4T. The stator is composed of 3-phase coils and a back yoke. The back yoke may cause nonlinearity of the magnetic field, however, it generates the high magnetic flux on the coils.

### B. Operating Principle

When these coils are excited, they are forced to move by Lorenz force. The mover is driven by the reaction force while the stator is fixed (see Fig. 6). And, the mover can be freely controlled by switching the 3-phase currents.

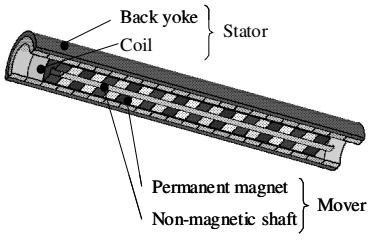


Fig. 4. Magnetic structure of the actuator

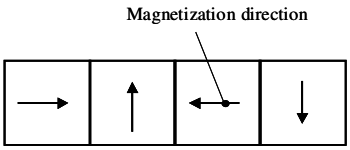


Fig. 5. Halbach array magnets

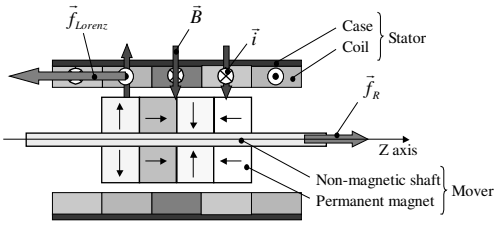


Fig. 6 Operating principle

## III. The Method of Analysis

The equations of the magnetic field and the electric circuit are coupled using the 3-D FEM, which are given by the magnetic vector potential $\boldsymbol{A}$ and the exciting current $I_0$ as follows [2]:

$$rot\,(\nu rot\boldsymbol{A}) = \boldsymbol{J}_0 + \nu_0 rot\boldsymbol{M} \tag{1}$$

$$E = V_0 - RI_0 - \frac{d\Psi}{dt} = 0 \tag{2}$$

$$\boldsymbol{J}_0 = \frac{n_c}{S_c} I_0 \boldsymbol{n}_s \tag{3}$$

where ν is the reluctivity, $\boldsymbol{J}_0$ is the exciting current density, $\nu_0$ is the reluctivity of the vacuum, $\boldsymbol{M}$ is the magnetization of permanent magnet, $V_0$ is the applied voltage, $R$ is the effective resistance, $\boldsymbol{\Psi}$ is the interlinkage flux of exciting coil. $n_c$ and $S_c$ are the number of turns and the cross-sectional area of the coil, respectively. And $\boldsymbol{n}_s$ is the unit vector along with the direction of exciting current.

The motion of the mover is described as follows.

$$M\frac{d^2z}{dt^2} + D\frac{dz}{dt} = F \mp F_s \tag{4}$$

where $M$ is the mass of the mover, $z$ is the displacement of the mover, $D$ is the viscous damping coefficient, $F$ is the electromagnetic force, and $F_s$ is the dynamic friction force.

## IV. Optimization of The Actuator

We have investigated the influence of geometrical parameters, two types of materials for the case, coil excitation method, and input current waves. Then, we have optimized the geometrical parameters and the driving system.

The fixed conditions are as follows. The external diameter is 30mm. The thickness of the back yoke is 2.5mm. And, the gap between coils and magnets is 1mm and the shaft diameter is 4mm. These are constrained dimensions for applying it to the arm of the android. Conditions of the analysis are shown in Table 1.

### A. Optimization of geometrical parameters

#### 1) Optimization of the magnet's pitch

The pitch of the arrayed magnets is optimized when the coil pitch is fixed in order to maximize the average thrust. Fig. 7 shows the simulation results of the thrust per unit length while the pitch of the arrayed magnet is changed from 2mm to 8mm with a step of 1mm. The input current for each coil is 0.7A. The number of turns of each coil is 525turns.

The largest thrust per unit length has been obtained at the magnet pitch of 6mm. Other parameters were also optimized according to the above process. As the result, the optimized geometry has been obtained as shown in Fig. 8.

#### 2) Influence of the case's materials

The magnetic circuit is shown in Fig. 9. The mover is driven by the magnetic flux density generated by the magnets' block of the mover. By exchanging the material of the case with pure iron, the leak of the magnetic flux density is decreased and more efficient magnetic circuit is obtained. We have compared the static thrust of the magnetic case with that of the non-magnetic case while the stroke of the mover is changed from 0 to 20mm with a step of 1mm under rectangular wave current (the effective value is 0.7A).

TABLE I
ANALYSIS CONDITIONS

| | |
|---|---|
| Effective voltage [V] | 3.5 |
| Number of turns [Turns] | 525 |
| Resistance [Ω] | 3.5 |
| Mass of mover [g] | 238 |
| Friction force [N] | 0.93 |
| Viscous damping coefficient [N•s/m] | 1.0 |

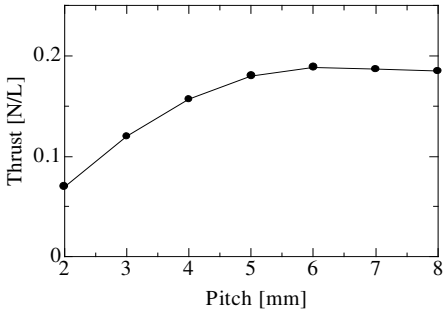


Fig. 7. Thrust vs. Magnet pitch

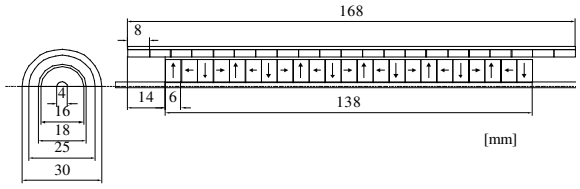


Fig. 8. Optimal geometry of proposed actuator (3-phase model)

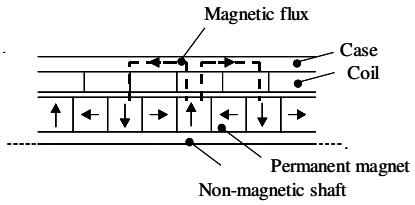


Fig. 9. Magnetic circuit of the actuator

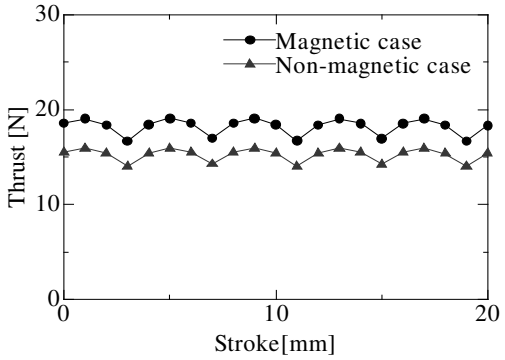


Fig. 10. Comparison of thrust characteristics

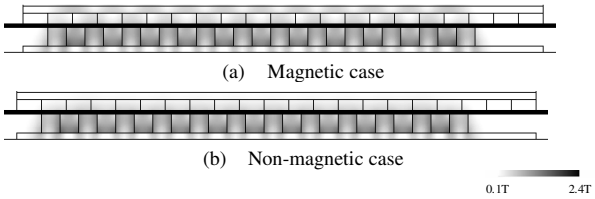


Fig. 11. Magnetic flux density distribution

The simulation results of both models are shown in Fig. 10. The maximum thrust, the average thrust and the ripple of the thrust of the magnetic case model are about 19.08N, 18.23N and 12.52%, respectively. The maximum thrust, the average thrust and the ripple of the thrust of the non-magnetic case model are about 15.91N, 15.23N and 11.85%, respectively. From these results, we have found that the magnetic case model is better than the non-magnetic case model. Each magnetic flux density distribution is shown in Fig. 11 with 0mm stroke. It shows that the maximum magnetic flux density of each coil is approximately 0.6T for the magnetic case model and that is approximately 0.45T for the non-magnetic case. In addition, the magnetic flux density of the magnetic case is about 0.65T and it is not saturated.

### B. Optimization of the driving system

#### 1) Influence of the coil excitation method to the thrust

We have also investigated influence of the number of coil excitation phase to the thrust and compared the thrust of the 3-phase coil excitation and that of the 2-phase coil excitation while the stroke of the mover is changed from 0 to 20mm with a step of 1mm with rectangular wave current (the effective value is 0.7A). The coil pitches of the 3-phase and the 2-phase models are 8 and 12mm, respectively.

The simulation results of both models are shown in Fig. 12. The average thrust and the ripple of the 3-phase model are approximately 18.23N and 12.52%, respectively. On the other hand, those of the 2-phase model are approximately 14.68N and 83.35%, respectively. From these results, we have found that the 3-phase model is extremely better than the 2-phase model.

*2) Influence of the waveform of coil excitation current to the thrust*

We have investigated the influences of the waveform of coil excitation current on to the thrust in the 3-phase model. Concretely, we have compared the static thrust of rectangular wave current with that of sinusoidal current while the mover stroke is changed from 0 to 20mm with a step of 1mm. Fig. 13 shows the input rectangular and sinusoidal wave currents (the effective value is 0.7A).

The static thrust characteristics of both input current waveforms are shown in Fig. 14. When the input current waveform of the 3-phase sinusoidal wave is applied, the average thrust and the ripple are about 19.89N and 2.09%, respectively.

We have compared the dynamic performances while the mover moves from 0 to 8mm with the 3-phase excitation by the sinusoidal and rectangular input current (the effective current $I_e$ is 0.7[A]). It is shown in Fig. 15. Table 2 shows the conditions for the simulation. The maximum velocity of the rectangular wave current is about 0.652m/s. That of the sinusoidal wave current is about 0.708m/s.

The average power consumption and the average efficiency are computed as follows.

$$W = \int_{t_s}^{t_e} i \cdot V dt \tag{5}$$

$$\eta = \frac{\int_{x_s}^{x_e} f_R \cdot v dx}{W} \tag{6}$$

The average power consumption and the average efficiency of the rectangular wave current are about 7.7W and 69.5%, respectively. And, those of the sinusoidal wave current are about 7.55W and 85.9%, respectively. These results show the better effectiveness of the 3-phase sinusoidal excitation.

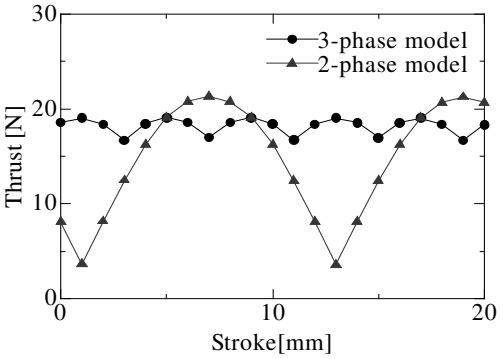


Fig. 12. Comparison of thrust characteristics

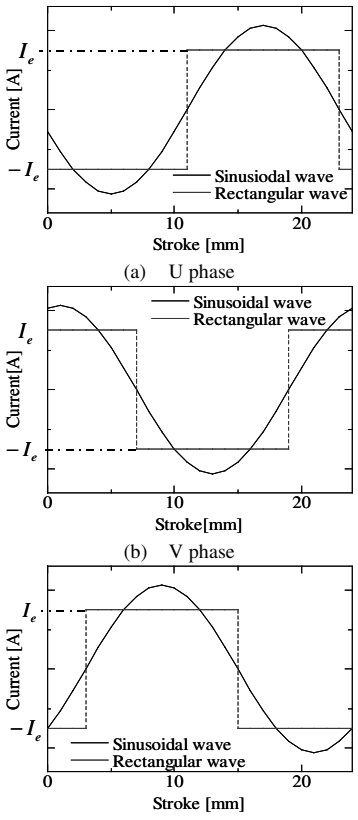


Fig. 13 3-phase sinusoidal and rectangular currents

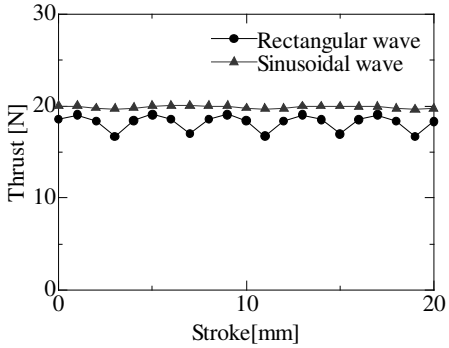


Fig. 14 Comparison of thrust characteristics

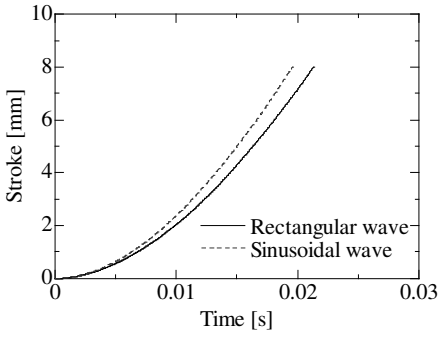


Fig. 15 Response characteristics

## V. Comparison with Conventional Synchronous Motors

In order to confirm the effectiveness of the Halbach array magnets, we have compared with the conventional linear synchronous motor (so called shaft motor), which operating principle is similar to our actuator. The mover of the shaft motor consists of magnets that are arranged with opposite magnetization directions side by side and generate the high magnetic flux above their boundaries. Under the same size and the conditions of analysis, we have simulated the static and dynamic performances by the 3-D FEM.

The static thrust characteristic of both models is shown in Fig. 17. The maximum thrust, the average thrust and the ripple of the shaft motor are approximately 15.45N (about 30% weaker than the proposed actuator), 15.22N (about 30% weaker) and 2.22%, respectively. The magnetic flux density distribution of the shaft motor is shown in Fig. 18 with 0mm stroke. The maximum magnetic flux density of each coil is approximately 0.5T.

Dynamic performance, or response characteristics, of those actuators is shown in Fig. 19. The response time of the proposed actuator and the shaft motor is 0.0192s and 0.0273s, respectively. That is, our actuator is about 30% better than the shaft motor.

TABLE II
Discretization Data and CPU Time

| | |
|---|---|
| Number of elements | 275,520 |
| Number of node | 69,785 |
| Number of edge | 391,336 |
| Number of unknown variables | 391,283 |
| Number of time steps | 413 |
| Total CPU time (hours) | 24.2 |

(Intel Pentium 4, CPU 3.00GHz)

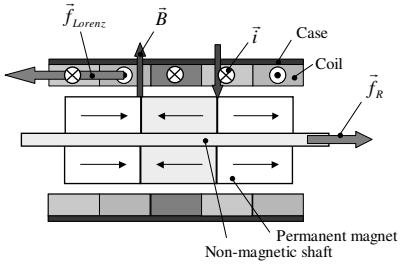


Fig. 16 Operating principle of the shaft motor

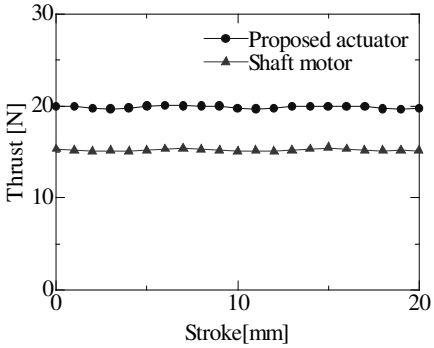


Fig. 17 Comparison of the thrust characteristics

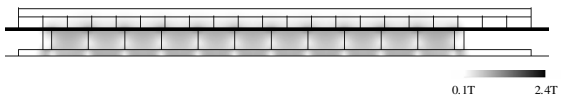


Fig. 18 Magnetic flux density distribution of the shaft motor

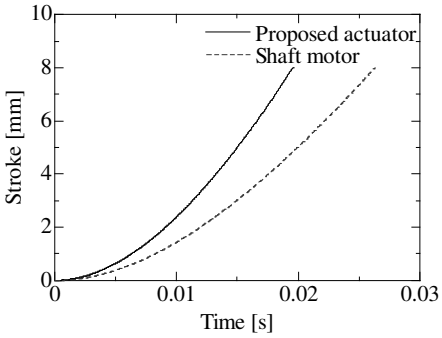


Fig. 19 Response characteristics

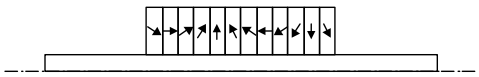

Fig. 20 Subdivided model

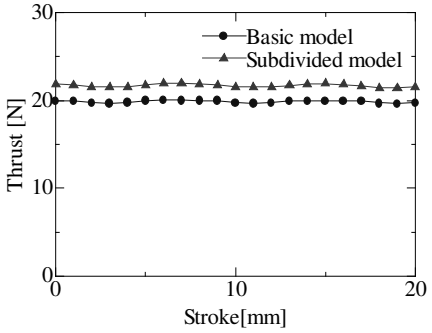


Fig. 21 Comparison of the thrust characteristics

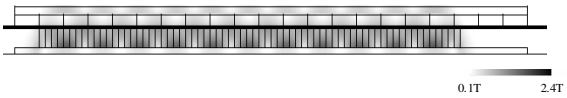


Fig. 22 Magnetic flux density distribution

## VI. Influence of Subdivision of The Halbach Array

### A. Subdivided model of the Halbach array

The proposed Halbach array is not ideal. By subdividing the array, we can improve the performance. This section shows the additional simulations for improving the actuators. Fig. 20 shows the subdivided Halbach array.

### B. *The results of analysis*

The static thrust characteristic of the subdivided model is shown in Fig. 21. The maximum thrust and the average thrust of the subdivided model are approximately 21.99N (about 9.6% better than the previous basic model) and 21.69N (about 9.0% better), respectively. The magnetic flux density distribution is shown in Fig. 22 with 0mm stroke. The maximum magnetic flux density of each coil is approximately 0.63T. This is about 5% better than the basic model.

## VII. DEVELOPMENT OF THE PROTOTYPE

To verify the simulation results by the 3-D EFM, we have developed a prototype based on the basic model described in Section II. Fig. 23 and 24 show the prototype and the control system, respectively. Fig. 25 shows the comparison between the simulated and measured waveforms of the 3-phase current in the prototype. As shown in the figure, both results match each other very well although there is small difference (about 7.19% at U phase) because of the experimental error. This error is due to assembling precision of a prototype.

Fig. 26 shows the comparison between simulated and measured in the response that is represented as relation between various times and the stroke. The results also match each other very well. Here, the maximum velocity of the prototype is 0.71m/s. Through these results, we could verify the reliability of the 3-D EFM and the performance of the new linear actuator based on the Halbach magnet array.

## VIII. CONCLUSION

Robots are going to be more complicated and they require more flexible and powerful actuators. With respect to the development of the actuators, we have proposed the new structure of linear actuator, simulated the performance by the 3-D FEM, and verified the reliability of the simulation by building the prototype.

The developed linear actuator is 30% better in the thrust and 40% better in the response comparing with the shaft motor that is the most powerful linear actuator. As shown in Section VI, it is possible to improve the performance by subdividing the Halbach array.

Our next step is to develop new prototypes base on the new Halbach array and flexible control software as robot actuators. By controlling the voltage and current for driving the actuator, we consider it will be powerful and flexible enough for various robots.

## REFERENCES


[1] H. Ishiguro, "Scientific issues concerning androids," International Journal of Robotics Research, Vol. 26, No. 1, 2007, pp. 105-117.

[2] K. Hirata, T. Yamamoto, T. Yamaguchi, Y. Kawase and Y. Hasegawa, "Dynamic Analysis Method of Two-Dimensional Linear Oscillatory Actuator Employing Finite Element Method", IEEE Transaction on Magnetics, VOL.43, No.4, pp.1441-1444, 2007.04

[3] K. Halbach, "Application of permanent magnets in accelerators and electron storage rings," Journal of Applied Physics, vol.57, 1985, pp.3605-3608.

[4] Z.O. Zhu and D. Howe, "Halbach permanent magnet machines, and applications: A Review, " IEEJ Proceedings of Electrical Power Applications Vol.148, No.4, 2001, pp.299-308.


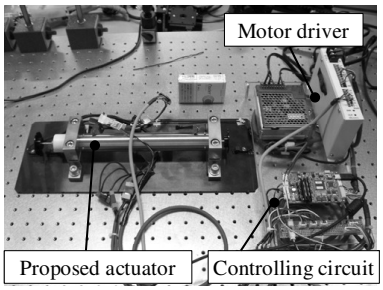


Fig. 23 The prototype

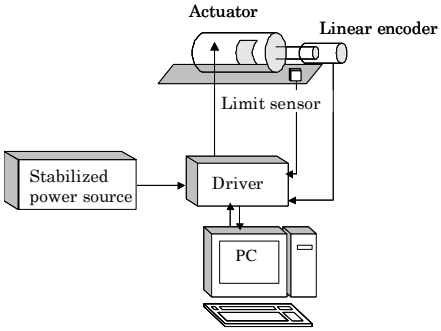


Fig. 24 System configuration of the prototype

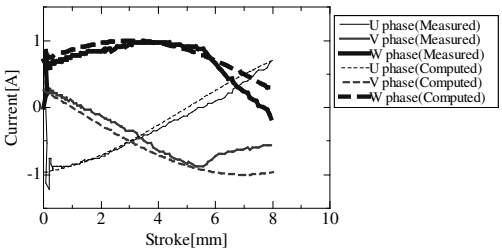


Fig. 25 Stroke v.s. Current

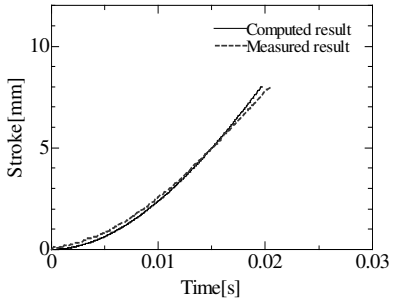


Fig. 26 Time v.s. Stroke